Chinese Chemical Letters 34 (2023) 107292

Contents lists available at ScienceDirect

Chinese Chemical Letters

journal homepage: www.elsevier.com/locate/cclet

A hybrid ambipolar synaptic transistor emulating multiplexed neurotransmission for motivation control and experience-dependent learning

Zhipeng Xu[1], Yao Ni[1], Hong Han, Huanhuan Wei, Lu Liu, Shuo Zhang, Hao Huang, Wentao Xu*

Institute of Optoelectronic Thin Film Devices and Technology, Key Laboratory of Optoelectronic Thin Film Devices and Technology of Tianjin, College of Electrical Information and Optical Engineering, National Institute for Advanced Materials, Nankai University, Tianjin 300350, China

ARTICLE INFO

Article history:
Received 15 January 2022
Revised 16 February 2022
Accepted 3 March 2022
Available online 7 March 2022

Keywords:
Hybrid ambipolar
Artificial synapse
Dual excitatory channels
Fast-switching plasticity
Task-learning process

ABSTRACT

Artificial synapses with full synapse-like functionalities are of crucial importance for the implementation of neuromorphic computing and bioinspired intelligent systems. In particular, the development of artificial synapses with the capability to emulate multiplexed neural transmission is highly desirable, but remains challenging. In this work, we proposed a hybrid ambipolar synaptic transistor that combines two-dimensional (2D) molybdenum disulfide (MoS_2) sheet and crystalline one-dimensional (1D) poly(3-hexylthiophene-2,5-diyl) polymer nanowires (P3HT NWs) as dual excitatory channels. Essential synaptic functions, including excitatory postsynaptic current, paired-pulse facilitation, synaptic potentiation and depression, and dynamic filtering were emulated using the synaptic transistor. Benefitting from the dual excitatory channels of the synaptic transistor, the device achieved a fast switch between short-term and long-term memory by altering the charge carriers in the dual channels, *i.e.*, electrons and holes. This emulated the multiplexed neural transmission of different excitatory neurotransmitters, *e.g.*, dopamine and noradrenaline. The plasticity-switchable artificial synapse (PSAS) simulates the task-learning process of individuals under different motivations and the impact of success or failure on task learning and memory, which promises the potential to enable complex functionalities in future neuromorphic intelligent electronics.

The traditional von Neumann-based computing architecture requires a large amount of data transmission between physically separated central processing units and data storage units, which limits the efficiency for processing large quantities of complex data [1,2]. Neuromorphic electronics can quickly recognize patterns, tasks, and memorize or recall information with a very low energy consumption, and have been demonstrated great potential in brain-inspired computing [3–8]. In a neuromorphic system, artificial synapses are the key functional elements for information transmission, processing and integration. The ceaseless advancement of neuromorphic computing requires further improvement in artificial synapses.

Current artificial synapses can realize basic synaptic functions in a single device [9–14]. Artificial synapses using low-dimensional materials including zero-dimensional quantum dots, one-dimensional (1D) nanowires, nanotubes and nanoribbons, and two-dimensional (2D) nanosheets and films have been reported in recent years. Two-dimensional transition metal dichalcogenides (TMDCs) and organic semiconductors have been further employed for plasticity-tunable artificial synapses [15–21]. 2D $MoTe_2$-based artificial synaptic arrays on silicon-rich silicon nitride (sr-SiN_x) substrate exhibited device-to-device and cycle-to-cycle stability with high on/off ratio and conductance update linearity [22]. A synaptic transistor based on monolayer MoS_2 and an intentionally Na^+ diffused SiO_2 layer can work efficiently at a high temperature. This provided a promising strategy for high-temperature neuromorphic applications [23]. Benefitting from the special design of the 2D conjugated polymer (CP) with nanoscale-segregated 'polka dot'-structured crystalline phases and adjacent amorphous phases, 2D CP-based synaptic transistor emulated the different receptors of *N*-methyl-D-aspartate (NMDA) and α-amino-3–hydroxy-5-methyl-4-isoxazole propionic acid (AMPA) on the postsynaptic membrane [24].

---

* Corresponding author.
E-mail address: wentao@nankai.edu.cn (W. Xu).

[1] These authors contributed equally to this work.

https://doi.org/10.1016/j.cclet.2022.03.015

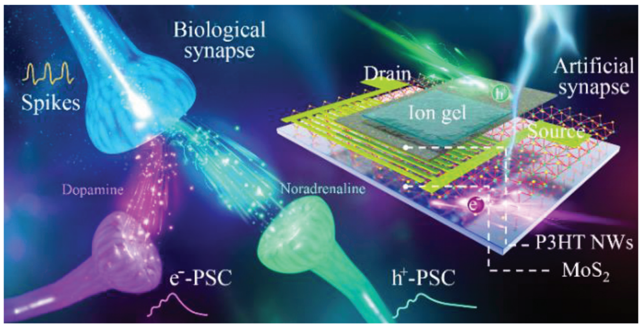

Fig. 1. Schematic of biological synapse and the PSAS with two independent channels for holes and electrons transporting. The electrons and holes transporting in the dual channels emulate two kinds of neurotransmitters, *e.g.*, dopamine and noradrenaline, in the synaptic cleft.

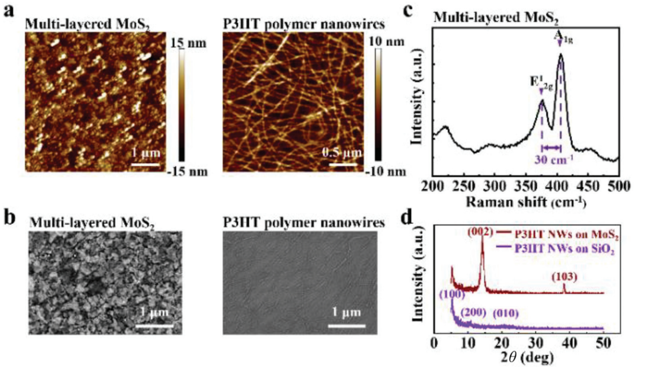

Fig. 2. (a) AFM images of the multi-layered MoS_2 and P3HT polymer nanowires. (b) SEM images of multi-layered MoS_2 and P3HT polymer nanowires. (c) Room-temperature Raman spectra of the 2D MoS_2. (d) XRD patterns of P3HT NWs on SiO_2 or MoS_2.

These artificial synapses mostly used unipolar active materials to emulate the release of a single type of neurotransmitter. However, some higher forms of plasticity require more than one type of neurotransmitter in a synapse to achieve synergistic responses and to maintain biological homeostasis in complex environments [25–30]. For example, the neurotransmitters of dopamine and noradrenaline can function in an independent or coordinative manner to facilitate learning and maintain the states required for normal cognitive processes [31]. Thus, a plasticity-switchable artificial synapse (PSAS) emulating the multiplexed neurotransmission of different neurotransmitters with a fast-switch mechanism in response to a complex external environment is highly desirable. Here, we propose a PSAS based on a hybrid ambipolar synaptic transistor that emulates the multiplexed neural transmission of different excitatory neurotransmitters by changing the charge carriers to achieve the immediate switchable short-/long-term plasticity. The PSAS features parallel channels with n-type multi-layered MoS_2 and p-type crystalline P3HT polymer nanowires. The parallel channels serve as paths of different charge carriers, *i.e.*, electrons and holes, emulating the switching and competition between two kinds of excitatory neurotransmitters, *e.g.*, dopamine and noradrenaline in a biological synapse. Synapse-like functions, including excitatory postsynaptic current, paired-pulse facilitation, synaptic potentiation and depression, and dynamic filtering were emulated. Furthermore, we quantified the impact of conductance state updates with different synaptic weight ranges and linearities on pattern training/recognition. Inspired by Atkinson's achievement motivation theory, we simulated the task learning process of individuals with different motivations and the backward influence of success and failure experiences. The dual-channel strategy facilitates multiplexed neural transmission, which promises potential applications in bio-inspired and bio-integrated electronics.

The transportation of electrons or holes in separated channels emulates the release of different neurotransmitters, *e.g.*, dopamine and noradrenaline, in a biological synapse (Fig. 1). The PSAS with MoS_2/P3HT NWs-based dual-transmission channels was fabricated on a SiO_2 substrate. The source and drain metal electrodes were deposited between the MoS_2 layer and the P3HT NWs layer. A top ion-gate is coupled with the MoS_2/P3HT NWs-based dual channels by 1-ethyl-3-methylimidazolium (EMIM) cations and trifluoromethylsulfonyl (TFSI) anions. The MoS_2 film features a common lamellar crystal, whereas the self-assembled P3HT chains aggregate to form polymer nanowires by solvent engineering (Figs. 2a and b) [32–34]. The thicknesses of MoS_2 and P3HT NWs layers are 9 nm and 20 nm, respectively (Fig. S2 in Supporting information).

Raman spectrum of the CVD-grown MoS_2 film shows a frequency difference of ~30 cm^{-1} between the $E^1{}_{2g}$ and A_{1g} vibration modes, in agreement with the multi-layered flakes (Fig. 2c) [35]. In the high-resolution X-ray photoelectron spectroscopy (XPS) spectra of the MoS_2 and MoS_2/P3HT NWs thin films (Fig. S3 in Supporting information), the Mo 3d peak is split into two peaks that can be attributed to the presence of the doublet of Mo $3d_{5/2}$ and Mo $3d_{3/2}$. The S 2p peak is decomposed into two peaks corresponding to the S $2p_{1/2}$ and S $2p_{3/2}$. In X-ray diffraction (XRD) pattern of P3HT polymer nanowires, the intensity of the diffraction peak at lamellar (100) orientation ($2\theta = 5.3°$) is very strong, whereas the peak of π-π overlapping (010) orientation ($2\theta = 23°$) was undetectable (Fig. 2d) [36]. This result suggests "edge-on" orientation of P3HT molecules with the conjugation plane perpendicular to the surface of the SiO_2 substrate [37–39]. The XRD pattern of MoS_2 film exhibits distinct peaks of (002) and (103) orientations [16].

Presynaptic inputs trigger ionic polarization in ion gel, inducing additional charge carriers in conductive channels. This process is analogous to the release of neurotransmitters in the synaptic cleft to induce a postsynaptic current (PSC) in the dendrite of postneuron. Two independent channels allow transportation of different charge carriers, *i.e.*, electrons in n-type MoS_2 channel and holes in p-type P3HT NWs channel, depending on the polarity of voltage inputs (Fig. 3a and Fig. S4 in Supporting information). Therefore, the release process of two kinds of excitatory neurotransmitters, *i.e.*, dopamine and noradrenaline are emulated. The transmission channels of different charge carriers more realistically emulate the transmission channels of multiple neurotransmitters in a neuron. The transfer of charge carriers can be adjusted by altering the reading voltage, which emulates the cell membrane potential of the post-neuron. Positive presynaptic inputs (6 V) cause cation accumulation at the surface of the MoS_2/P3HT NWs-based dual channels, and then induce electrons in MoS_2 channel. Such a process makes the channel open for electron-dominated transmission, and emulates the transmission of dopamine in the synaptic cleft. Otherwise, negative presynaptic inputs (−5 V) cause anion accumulation at the surface of the dual channels and induce holes in P3HT NWs channel to open P3HT channel for hole-dominated transmission, which emulates the transmission of noradrenaline. Under the reading voltages with different polarity (0.02 V or −0.02 V), the device exhibits synaptic potentiation (Fig. 3b). The changes in postsynaptic current (ΔPSC) of the four devices triggered by presynaptic spike demonstrated the repeatability of the device (Fig. S5 in Supporting information).

Short-term plasticity (STP) and long-term plasticity (LTP) form the foundation for neural experience acquisition [40,41]. The synaptic plasticity can be tuned by adjusting the number, frequency, and amplitude of presynaptic spikes. Our PSAS emulated paired-pulse facilitation (PPF) by applying a pair of identical

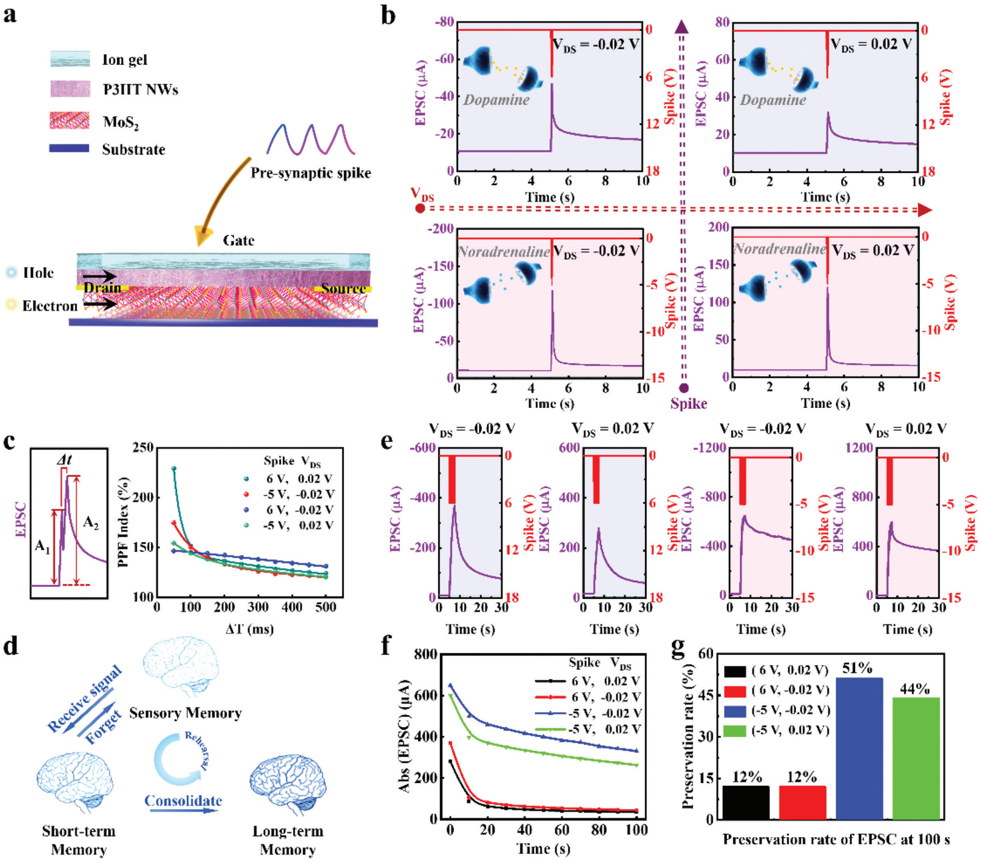

Fig. 3. The designed PSAS emulates the multiple plasticity dominated by dopamine and noradrenaline and the switchable short-/long-term plasticity. (a) Schematic illustration the PSAS with two independent channels (one for hole transport and the other for electron transport). When presynaptic spikes are applied to the ion gel, the mobile ions move in the electrical field in a manner analogous to neurotransmitters in the synaptic cleft that later induce a PSC in the dendrite by contacting the postsynaptic membrane. PSC composed of electrons or holes is generated in the MoS_2 or P3HT NWs layer in response to two kinds of opposite presynaptic spikes and is delivered to a postneuron through connections to the metal pad. (b) PSCs for PSAS triggered once by different external spikes (6 or −5 V, 50 ms), under different reading voltages (0.02 V and −0.02 V). (c) PPF index *vs.* time between successive spikes. (d) Schematic of rehearsal memory process in biology. (e) PSCs for PSAS triggered 30 times by different external spikes (6 or −5 V, 50 ms), under different reading voltages (0.02 V and −0.02 V). (f) The retention EPSC in 100 s and (g) the preservation rate of EPSC at 100 s after PSAS was triggered by 30 times external spikes.

presynaptic spikes [10]. Two consecutive presynaptic spikes (6 or −5 V, 50 ms) were applied to the gate electrode under two different cell membrane potentials of 0.02 V and −0.02 V, and the interval time (Δt) between the two spikes ranged from 50 ms to 500 ms (Fig. S6 in Supporting information). When the first spike was applied to the gate electrode, the polarized ions were transferred to the interface between ion gel and conductive channel, inducing charge carriers in conductive channel. Then, the ions were redistributed after the first spike was withdrawn. However, the second spike arrived before all ions returned to their equilibrium sites, so more ions accumulated in the interface between ion gel and the channel, thereby inducing more charge carriers in the channel. Therefore, the second excitatory postsynaptic current (EPSC) was larger than the first one, and the amplitude of the second EPSC (A_2) could reach to ~229.2% of the first EPSC (A_1). The experimental PPF indexes ($100\% \times A_2/A_1$) fitted well with the double exponential function $C_1\exp(-\Delta t/\tau_1)+C_2\exp(-\Delta t/\tau_2)+1$, where Δt is the spike interval of the two spikes, C_1 (C_2) and τ_1 (τ_2) are the initial facilitation magnitude and characteristic relaxation time of the rapid (slow) decay, respectively. PPF index is related to the Δt between two presynaptic spikes. As shown in Fig. 3c, the PPF index of the PSAS decreased gradually as Δt increased, analogous to forgetting curves.

Enhanced memory has been achieved after rehearsal processes (Fig. 3d). We recorded the EPSC within 100 s after the removal of external spikes and calculated the preservation rate at 100 s (Figs. 3e-g). The results showed that 30 consecutive spikes of 6 V facilitated the increase of electron-induced EPSCs (e^--PSC) and showed 12% of the peak value at 100 s. However, when 30 spikes of −5 V were applied, the hole-induced EPSCs (h^+-PSC) preserved ~50% of the peak current at 100 s. The hole-induced excitatory postsynaptic current in the P3HT NWs channel had a higher preservation rate, which is due to the high crystallinity of the P3HT NWs film. The doped ions trapped in the crystalline P3HT NWs film cannot easily diffuse out, so the holes still remained in the conductive channel after the spikes were removed. This is consistent with previous reports [32,39].

Spike-frequency-dependent plasticity (SFDP) is considered as a basic learning rule correlating with learning, associative memory, and forgetting [42]. Typical SFDP was emulated under the positive and negative reading voltages (Fig. S7 in Supporting information). The PSCs were notably enhanced as the frequency of spikes increased. Positive inputs enhanced e^--PSC in MoS_2 channel as the frequency of spikes increased because high-rate spikes strengthen the accumulation of cations. Analogously, the hole-induced PSCs increased as the negative input frequency increased. The dependence of the PSC on the spike frequency could fit well with the high-pass filtering characteristic of biological synapses [43,44]. The high-pass filter allows signals with frequencies higher than a certain cut-off frequency to pass, while greatly attenuating lower-frequency signals. This can remove unnecessary low-frequency components in the signal or remove low-frequency

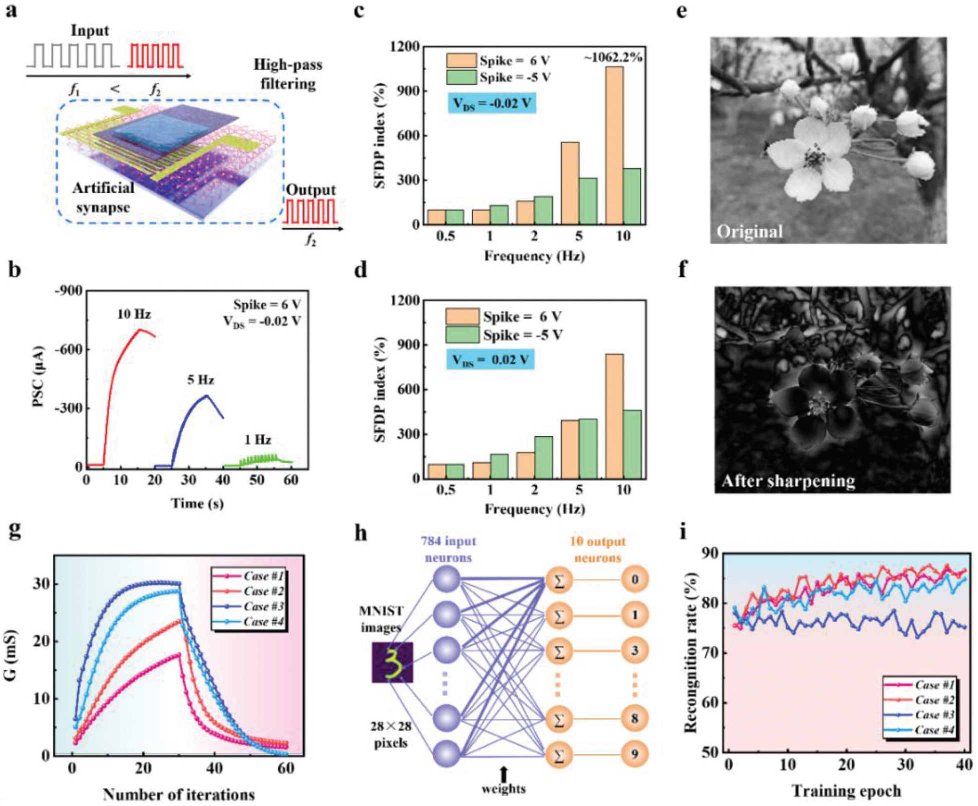

Fig. 4. The filtering behavior of PSAS and recognition simulation for MNIST patterns. (a) Schematic diagram of PSAS-based high-pass filtering function. (b) SFDP triggered by consecutive spikes with frequencies of 1, 5 and 10 Hz. (c, d) SFDP index ($A_n/A_1 \times 100\%$) triggered by a series of spikes (spike = 6 or −5 V), according to spike frequency from 0.5 to 10 Hz, under different reading voltages (0.02 V and −0.02 V). (e) The original image of the flower. (f) The image of the flower after sharpening with the high-pass filtering function at the cut-off frequency of 7.005 Hz. (g) Analog weight update. The continuous increase of channel conductance G caused by a series of repeated SPSs of 6 V or SNSs of −5 V, and the decrease of G triggered by a series of repeated ISNSs of −2.5 V or ISPSs of 3 V. (h) Neuron network structure for pattern recognition. (i) Estimated recognition rate for the MNIST patterns as a function of the training number according to four cases (#1, #2, #3 and #4).

interference. Fig. 4a shows the schematic diagram of a PSAS-based high-pass filter for signal processing. The PSC amplitude increased with the frequency increased, and increased dramatically when the frequency exceeds 5 Hz (Fig. 4b). The SFDP index ($100\% \times A_n/A_1$) was plotted as a function of the frequency of presynaptic spike (Figs. 4c and d). The maximum index could reach to $\sim$1062.2% when the frequency was up to 10 Hz. In order to show the high-pass filtering function of PSAS more vividly, an image of a flower was used to show the high-pass filtering process (Figs. 4e and f). For the simulation, the curve of SFDP index was fitted with the sigmoidal function $H(f) = (a_1 - a_2)/(1 + (f/f_C)^p) + a_2$, which was analogous to the high-pass filter characteristic observed in biological synapse [44]. The fitting gave rise to the value of 7.005 Hz for the cut-off frequency (f_C) (Fig. S8 in Supporting information). When the f_C of 7.005 Hz was used for high-pass filtering, the image could be sharpened. Compared with the original image, the edge details in the image have been significantly improved. This indicated our PSAS has the potential to serve as a dynamic high-pass filter for signal processing.

Our PSAS device can mimic synaptic potentiation and depression under both positive and negative reading voltages (0.02 V and −0.02 V), corresponding to four cases. The PSAS devices were treated with equal numbers of sufficient positive spikes (SPSs) (6 V, 50 ms) (case #1 and #2, Fig. S9 in Supporting information) or sufficient negative spikes (SNSs) (−5 V, 50 ms) (case #3 and #4, Fig. S9) to induce excitatory neurotransmitters. Then, the potentiated devices were treated using 30 repeated insufficient negative spikes (ISNSs) (−2.5 V, 50 ms) or 30 repeated insufficient positive spikes (ISPSs) (3 V, 50 ms) to depress the excitement. With an appropriate number of consecutive spikes with a fixed voltage, the continuous updates of channel conductance (G) of the four cases were calculated (Fig. 4g). This availability of several flexible regulatory options increased the tunability of storage states of PSAS in neuromorphic computing networks [45,46].

To evaluate the learning capability of PSAS, the Modified National Institute of Standards and Technology (MNIST) pattern recognition was simulated. A neural network was constructed according to the electrical properties of the synaptic transistor to perform supervised learning with backpropagation of the MNIST dataset. For the simulation, 28×28 MNIST data were unwrapped to 1×784 row vectors to perform vector matrix multiplication. A two-layer network consists of an input layer, an output one, and a connective weight matrix, which are composed of 784 input neurons, and 10 output neurons, respectively (Fig. 4h). 10 output neurons correspond to 10 classes of digits (0–9). The channel conductance change was used as the weight update for executing the backpropagation algorithm (Fig. S10 in Supporting information). The recognition accuracies of the simulated networks after each training epoch are plotted in Fig. 4i. The synaptic weight update speed dominates the convergence speed. Therefore, after the first training iteration, the recognition accuracies of case #3 and #4 can reach to 78%, which were higher than those of case #1 and #2 due to the larger synaptic weight update range. However, after multiple trainings, the main parameter that affects the recognition accuracy is converted into the linearity. As training epochs increased, recognition rates of cases #1 and #2 improved, with the highest recognition rate up to 86.6% after 40 training epochs. By selecting an appropriate recognition mode, our PSAS-based neural network can

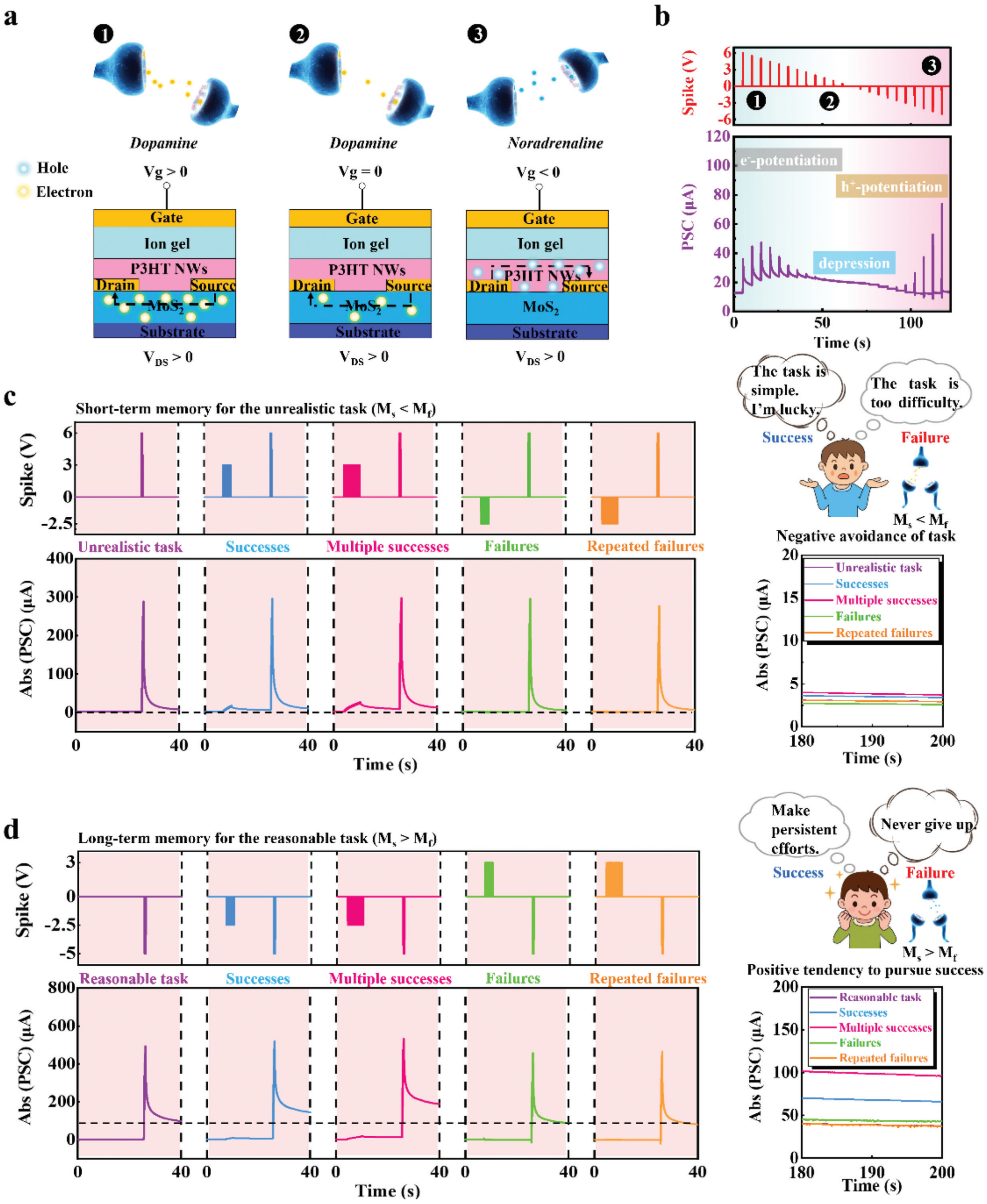

Fig. 5. Simulation of selective release of dopamine and norepinephrine, and the simulation of Atkinson's achievement motivation theory. (a, b) The spike-voltage dependent current characteristics (from positive to negative spikes) at the reading voltage of 0.02 V. Schematic of transition and transformation of two kinds of excitatory neurotransmitters in the synaptic cleft to illustrate the transition from dopamine excitation to noradrenaline inhibition, and then to noradrenaline re-excitation. Using the dual channels of the PSAS device, it simulates the impact of individual achievement motivation differences on task learning, and the impact of success and failure on individuals. (c) If $M_s < M_f$, the result is a negative avoidance of task. These individuals will choose the unrealistic task. Furthermore, both failure and success in previous experiential learning has a weak influence on the subsequent task learning. (d) Persons in whom the motivation to achieve success is stronger than the motive to avoid failure ($M_s > M_f$) should prefer reasonable tasks of intermediate difficulty. Both success and failure can have a positive impact on their task learning.

meet different requirements for identification speed and accuracy in complex recognition scenarios. All in all, the higher accuracy is ascribed to better linearity and relatively higher synaptic weight range in the potentiation and inhibition trends of PSAS device (Fig. S9).

Release of the two neurotransmitters yields competition. When the applied positive spike was sufficient, the PSAS emulated the release of a large amount of dopamine. As the amplitude of the spike gradually reduced to 0, the quantity of dopamine decreased. Once the spike became negative, more noradrenaline was injected into the postsynaptic membrane to replace dopamine as the major neurotransmitter (Figs. 5a and b, Fig. S11 in Supporting information). When presynaptic spikes were applied separately, whether they were three consecutive 6 V or −5 V presynaptic spikes, the device exhibited excitatory postsynaptic current, which reflects the dual excitatory plasticity (Fig. S12 in Supporting information). However, when different presynaptic spikes were applied simultaneously, the resulting postsynaptic current is a smaller inhibitory current; this phenomenon is due to the combination of electrons and holes in the dual channels, which makes the effective charge carriers in the channel were decreased. Therefore, the PSAS realized the selective release and competition of different excitatory neurotransmitters.

Under negative spikes, larger amounts of holes are induced in P3HT NWs, while smaller amounts of holes can be induced in MoS_2 film under positive spikes. This can result in the changes in surface potential of the film, and further affect the threshold of our synaptic device (Figs. S13 and S14 in Supporting information). Thus, PSCs under different pre-stimulations also have a greater difference (Figs. S11 and S15 in Supporting information). By applying different external interventions and changing the polarity of presynaptic spikes, our devices can imitate Atkinson's theory of achievement motivation [47]. Atkinson pointed out that people's motivation for task learning can be classified into two types, namely the motivation to achieve success (M_s) and the motivation to avoid failure (M_f). Compared with those who have stronger motivation to avoid failure ($M_s < M_f$), people with stronger motivation to achieve success ($M_s > M_f$) usually have stronger experience-dependent plasticity and show more efficiency in performing tasks. In addition, success and failure experiences can also affect task learning. Here, our PSAS device simulates the task learning and memory of people when $M_s < M_f$ through electron-dominated transmission. A series of positive pulse inputs are applied to simulate task learning under $M_s < M_f$, and the situation of task memory is judged by the resultant PSC. In this way, both failure (expressed by positive pulses) and success (expressed by negative pulses) in previous experiential learning have a weak influence on the subsequent task learning (Fig. 5c). On the contrary, a series of negative pulse inputs are applied to simulate task learning under $M_s > M_f$. Different from the negative avoidance tendency, success (corresponding to negative pulses) in previous experiential learning can further strengthen their learning memory. Moreover, with the success number increased, the later learning efficiency is higher with a stronger memory ability. However, the adverse impact of the failure experience (corresponding to positive pulses) on the later stage is kept within a controllable value (Fig. 5d).

In conclusion, we fabricated a hybrid ambipolar artificial synapse that combines n-type multi-layered MoS_2 and crystalline p-type P3HT polymer nanowires to emulate the selective release and competition of different excitatory neurotransmitters, *e.g.,* dopamine and noradrenaline. The dual channels based on MoS_2/P3HT NWs enable precise regulation on our PSAS device by applying external spikes to alter different charge carriers and implement the fast switchable short-/long-term plasticity. Synaptic behaviors, including excitatory postsynaptic current, pair-pulse facilitation, synaptic potentiation and depression, and dynamic filtering have been mimicked. Furthermore, we have clarified the correlation between pattern training/recognition and the conductance state updates with different synaptic weight ranges and linearities. Interestingly, using the dual channels of the PSAS device, we simulated the task-learning process of individuals with different achievement motivations, and the backward influence of success and failure experiences on individuals. The plasticity-switchable artificial synapse with dual-channeled transmission provides a new way to design future neuromorphic intelligent electronics.

Declaration of competing interest

The authors declare that they have no known competing financial interests or personal relationships that could have appeared to influence the work reported in this paper.

Acknowledgments

This work was supported by the National Science Fund for Distinguished Young Scholars of China (No. T2125005), the Tianjin Science Foundation for Distinguished Young Scholars (No. 19JCJQJC61000), and the Shenzhen Science and Technology Project (No. JCYJ20210324121002008).

Supplementary materials

Supplementary material associated with this article can be found, in the online version, at doi:10.1016/j.cclet.2022.03.015.

References

[1] H.L. Park, Y. Lee, N. Kim, et al., Adv. Mater. 32 (2020) e1903558.
[2] S. Dai, Y. Zhao, Y. Wang, et al., Adv. Funct. Mater. 29 (2019) 1903700.
[3] Y. Kim, A. Chortos, W. Xu, et al., Science 360 (2018) 998–1003.
[4] C. Wu, T.W. Kim, H.Y. Choi, et al., Nat. Commun. 8 (2017) 752.
[5] K.M. Song, J.S. Jeong, B. Pan, et al., Nat. Electron. 3 (2020) 148–155.
[6] Y. van de Burgt, E. Lubberman, E.J. Fuller, et al., Nat. Mater. 16 (2017) 414–418.
[7] J.J. Yang, D.B. Strukov, D.R. Stewart, Nat. Nanotechnol. 8 (2013) 13–24.
[8] Y. Ni, Y. Wang, W. Xu, Small 17 (2021) 1905332.
[9] W. Xu, T.L. Nguyen, Y.T. Kim, et al., Nano Energy 48 (2018) 575–581.
[10] W. Xu, S.Y. Min, H. Hwang, et al., Sci. Adv. 2 (2016) e1501326.
[11] L. Liu, B. Cui, W. Xu, et al., J. Ind. Eng. Chem. 88 (2020) 111–116.
[12] H. Wei, H. Yu, J. Gong, et al., ACS Appl. Electron. Mater. 2 (2020) 316–322.
[13] J. Gao, Y. Zheng, W. Yu, et al., SmartMat 2 (2021) 88–98.
[14] F. Yang, L. Sun, Q. Duan, et al., SmartMat 2 (2021) 99–108.
[15] H.S. Lee, S.W. Min, M.K. Park, et al., Small 8 (2012) 3111–3115.
[16] Y. Huang, F. Zhuge, J. Hou, et al., ACS Nano 12 (2018) 4062–4073.
[17] S. Bertolazzi, D. Krasnozhon, A. Kis, ACS Nano 7 (2013) 3246–3252.
[18] N. Myoung, K. Seo, S.J. Lee, et al., ACS Nano 7 (2013) 7021–7027.
[19] Q.A. Vu, H. Kim, V.L. Nguyen, et al., Adv. Mater. 29 (2017) 1703363.
[20] S. Wang, C. Chen, Z. Yu, et al., Adv. Mater. 31 (2019) e1806227.
[21] J. Sun, Y. Choi, Y.J. Choi, et al., Adv. Mater. 31 (2019) e1803831.
[22] D. Xiang, T. Liu, X. Zhang, et al., Nano Lett. 21 (2021) 3557–3565.
[23] B. Wang, X. Wang, E. Wang, et al., Nano Lett. 21 (2021) 10400–10408.
[24] H. Han, F. Ge, M. Ma, et al., Nanoscale Horiz. 5 (2020) 1324–1331.
[25] J. Li, Q. Duan, T. Zhang, et al., RSC Adv. 7 (2017) 43132–43140.
[26] X. Yan, L. Zhang, H. Chen, et al., Adv. Funct. Mater. 28 (2018) 1803728.
[27] X. Yan, J. Zhao, S. Liu, et al., Adv. Funct. Mater. 28 (2018) 1705320.
[28] X. Yan, Z. Zhou, J. Zhao, et al., Nano Res. 11 (2018) 1183–1192.
[29] D.J. Barker, D.H. Root, S. Zhang, et al., J. Chem. Neuroanat. 73 (2016) 33–42.
[30] P. Calabresi, B. Picconi, L. Parnetti, et al., Lancet Neurol. 5 (2006) 974–983.
[31] Y. Ranjbar-Slamloo, Z. Fazlali, Front. Mol. Neurosci. 12 (2019) 334.
[32] H. Han, Z. Xu, K. Guo, et al., Adv. Intell. Syst. 2 (2020) 1900176.
[33] L. Li, G. Lu, X. Yang, J. Mater. Chem. 18 (2008) 1984–1990.
[34] X. Gao, J.G. Liu, Y. Sun, et al., Chin. Chem. Lett. 24 (2013) 23–27.
[35] C. Lee, H. Yan, L.E. Brus, et al., ACS Nano 4 (2010) 2695–2700.
[36] Y.D. Park, H.S. Lee, Y.J. Choi, et al., Adv. Funct. Mater. 19 (2009) 1200–1206.
[37] R.Joseph Kline, M.D. McGehee, M.F. Toney, Nat. Mater. 5 (2006) 222–228.
[38] H. Yang, T.J. Shin, L. Yang, et al., Adv. Funct. Mater. 15 (2005) 671–676.
[39] G.T. Go, Y. Lee, D.G. Seo, et al., Adv. Intell. Syst. 2 (2020) 2000012.
[40] D.G. Seo, Y. Lee, G.T. Go, et al., Nano Energy 65 (2019) 104035.
[41] Y. Park, J.S. Lee, ACS Nano 11 (2017) 8962–8969.
[42] S.I. Kim, Y. Lee, M.H. Park, et al., Adv. Electron. Mater. 5 (2019) 1900008.
[43] L. Yin, W. Huang, R. Xiao, et al., Nano Lett. 20 (2020) 3378–3387.
[44] J. Zhang, Q. Shi, R. Wang, et al., InfoMat 3 (2021) 904–916.
[45] C.S. Yang, D.S. Shang, N. Liu, et al., Adv. Funct. Mater. 28 (2018) 1804170.
[46] J. Jang, S. Park, G.W. Burr, et al., IEEE Electron. Device Lett. 36 (2015) 457–459.
[47] J.W. Atkinson, J.R. Bastian, R.W. Earl, et al. , J. Abnorm. Soc. Psychol. 60 (1960) 27–36.